Dynamic simulations of traditional masonry materials at different loading rates using an enriched damage delay

Theory and practical applications

Li Piani, T.; Weerheijm, J.; Sluys, L. J.

DOI
10.1016/j.engfracmech.2019.106576

Publication date
2019

Document Version
Accepted author manuscript

Published in
Engineering Fracture Mechanics

Dynamic simulations of traditional masonry materials at different loading rates using an enriched damage delay: theory and practical applications

T. Li Piani[a,b,*], J. Weerheijm[a,b], L.J. Sluys[a]

[a] *TU Delft, Stevinweg 1, 2628 CN Delft, The Netherlands*
[b] *TNO, Ypenburgse Boslaan 2, 2496 ZA Den Haag, The Netherlands*

Abstract

A local damage model has been recently developed for the numerical simulation of the static behaviour of adobe bricks. Mesh insensitivity of the local model was obtained by generalizing the damage delay concept based on a Dirichlet boundary condition decomposition integrated in an implicit solver. The regularization properties of the model were proven before only in statics. In this study, mesh independence is demonstrated in dynamics analysing the problem of a cantilever bar uniaxially loaded at high deformation rates. Furthermore, the physical background of the delay formulation is interpreted regarding the main failure processes in compression exhibited by quasi brittle materials used in masonry. Two limitations of the model in correctly simulating the dynamic behaviour of masonry bricks have been observed. Corrections to the original damage delay formulation are proposed in this study. These enhance the capability of the model to address also distributed failure of traditional geo-materials and the inherent rate dependence also at high strain rate regimes. The improvements are demonstrated in this paper by means of numerical simulations of both theoretical tests and practical applications. These consist of experimental tests in compression recently performed by the authors at different strain rates, from statics to high velocity impact tests.

Keywords: Adobe; mesh dependence; quasi brittle and ductile materials; high velocity impact and strain rate; dynamic increase factor.

1. Introduction

Built heritage of the contemporary city is more and more exposed to dynamic hazards of different nature [1]. Not only natural events such as floods or earthquakes may happen but also man-made threats such as ballistic impacts

*Tiziano Li Piani
Email address: t.lipiani@tudelft.nl. This is a post print author's version of the article. (T. Li Piani)

and blast explosions concern governments around the world due to an increase of the terrorist threat in Europe [2]. Because of high amplitudes and strain rates induced locally on the target, these events can produce severe damage in structures made of quasi brittle materials such as concrete [3]. In fact, the response of softening geo-materials is highly sensitive to the applied rate of loading [4]. Therefore, the development of interpretative tools capable of addressing the dynamic behaviour of quasi brittle materials is of paramount importance nowadays [5].

In engineering software, numerical simulations of material failure often use a damage framework [6]. Continuum damage mechanics constitutes a pragmatic approach close to the physics of the material because it interprets failure as a progressive degradation of the elastic capacity of the material [7]. In fact, in quasi brittle materials failure starts when the first micro-cracks coalesce starting from voids or defects inside the material and bridge into a macro-crack which may cause the progressive loss of structural integrity [8].

However, the link between many damage models and the corresponding physical mechanisms aimed to be addressed still represents a controversial issue not fully solved [9]. This is also the case because damage models suffer from a numerical pathology which prevents objective evaluations of failure for different spatial discretizations [10, 11]. To solve this issue, so-called regularization algorithms are coupled to local damage models. As a result, extra functions must be implemented, sometimes at the cost of controversial physical interpretations for the inherent numerical parameters. This is often the case, e.g. for non local regularization models [9].

Local regularization algorithms may solve mesh dependence using rate dependent damage laws and thus constitute the closest approach to the physics of quasi brittle materials in dynamics [11]. Unfortunately, only a limited number of these algorithms are capable of fully regularizing the models [12]. The regularization properties of a particular local algorithm have been recently demonstrated in statics [13]. It integrates a-dimensional damage delay functions based on decomposition of Dirichlet boundary conditions into the constitutive equations of a local model for concrete and solved using an implicit solver. The regularization algorithm is based on the concept of a bounded rate of damage, which was originally applied for simulating delamination problems in composites materials [14]. However, this can constitute a valid approach also for cement or clay-based quasi brittle materials commonly used in masonry [15].

The model developed in [13] for static loadings is briefly presented in Section 2 of this paper. The aim of this study is twofold. The regularization properties of the model are herein analysed for the dynamic problem at high loading rates including inertia effects (Section 3). Furthermore, the original delay algorithm is modified. Its formulation is enriched with two new material and external conditions dependencies in Section 4. The modifications address the specific limitations observed in numerical simulations of the dynamic response of quasi brittle materials using the original formulation. The opportunity of the proposed solutions are interpreted in light of the theory on the dynamic behaviour of quasi brittle materials commonly used in masonry. For both cases, they are

firstly numerically demonstrated via simulations of theoretical problems and validated via numerical simulations of two real dynamic compression tests recently performed by the authors on different types of masonry bricks [16]. Many of these tests concerned the material characterization of adobe components, sun-dried mixtures made of silt, sand and clay. The numerical simulations of the model presented in [13] were aimed at addressing the static behaviour of this traditional material. Therefore the model was originally named "adobe delta damage model" [15].

2. The adobe delta damage model

The model developed in [13] is briefly presented in this section. This model adapts a damage delay algorithm originally developed for laminated composites [17] in a local damage framework recently modified for the dynamic assessment of concrete [3, 18]. Implementation of the model starts from the classical formulation for isotropic damage in eq.(1) [19]:

$$\underline{\sigma} = (1 - D)\underline{\tilde{\sigma}} \quad \text{with} \quad \underline{\tilde{\sigma}} = \underline{\underline{E}}\,\underline{\varepsilon} \ , \tag{1}$$

where $\underline{\tilde{\sigma}}$ is the effective stress vector, $\underline{\varepsilon}$ is the strain vector, $\underline{\underline{E}}$ the elastic stiffness matrix and D is the damage scalar, a parameter which ranges between 0 (integer material) and 1 (fully damaged material). Damage starts when the loading function ψ in eq.(2) becomes positive:

$$\psi = \varepsilon_{eq} - k_0 \ , \tag{2}$$

where ε_{eq} and k_0 are the equivalent strain and the damage initiation strain, respectively.

The thermodynamic variables of the material states are expressed as equivalent strains for compression crushing (ε_{eq_c}) and tensile cracking (ε_{eq_t}) [20]. A modified Drucker-Prager damage surface is represented, which is suitable for a wide range of pressure-dependent building materials [21]. The equivalent strains are expressed as a combination of normal (ε_{oct}) and tangential (γ_{oct}) strain components in the octahedral space:

$$\begin{cases} \varepsilon_{eq_t} = c_1\varepsilon_{oct} + c_2\gamma_{oct} \\ \varepsilon_{eq_c} = c_3\varepsilon_{oct} + c_4\gamma_{oct} \end{cases} \tag{3}$$

which are related to the first (I_ε) and second deviatoric (J_{ε_d}) invariants of strain as in eq.(4):

$$\begin{cases} \varepsilon_{oct} = \dfrac{1}{3}I_\varepsilon = \dfrac{\varepsilon_1 + \varepsilon_2 + \varepsilon_3}{3} \\ \gamma_{oct}^2 = -\dfrac{8}{3}J_{\varepsilon_d} = \dfrac{4}{9}[(\varepsilon_1 - \varepsilon_2)^2 + (\varepsilon_2 - \varepsilon_3)^2 + (\varepsilon_3 - \varepsilon_1)^2] \end{cases} \tag{4}$$

where ν is the Poisson's ratio and subscripts $_{1,2,3}$ denote a principal value.

Parameters $c_1 - c_4$ are related to the elastic constants of the material and translate the equivalent strains in the octahedral stress space. They are taken

equal as in [3], but also other options are available according to the material properties [15]:

$$\begin{cases} c_1 = \frac{1}{(1-2\nu)} \\ c_2 = \frac{1}{2(\sqrt{2}(1+\nu))} \\ c_3 = \frac{3}{5(1-2\nu)} \\ c_4 = \frac{3\sqrt{3}}{5(\sqrt{2}(1+\nu))} \end{cases} \tag{5}$$

Evolution of damage is directly related to the growth of two monotonic internal variables which account for the maximum equivalent strains reached during loading history in case of non-monotonic loadings. These are implemented separately for compression (k_c) and tension (k_t) according to [12]:

$$\begin{cases} k_c(i) = \max[\ \varepsilon_{eq_c}(1-r^\alpha), k_{0c}(\tau)] \quad \text{for all} \quad i \geqslant \tau \\ k_t(i) = \max[\ \varepsilon_{eq_t} r^\alpha, k_{0t}(\tau)] \quad \text{for all} \quad i \geqslant \tau \end{cases} \tag{6}$$

Where r is derived from the triaxiality factor proposed by Lee and Fenves [22] for multiaxial loading states, α is a constant set to 0.1 as in [5] and the mechanical parameters k_{0t} and k_{0c} are the damage initiation strains in tension and compression [23].

Two damage evolutions laws called for compression and tension are dependent on the damage initiation strains determined by the stress state of the integration point. These are rate-independent laws resulting from linear and exponential softening functions [24]:

$$d_{c,t} = 1 - \frac{1}{e^{a_{c,t}(k_{c,t} - k_{0_{c,t}})}} - \frac{k_{0_{c,t}}}{b_{c,t} k_{c,t}} \tag{7}$$

Where a and b are non dimensional parameters.

For both compression and tension, eq.(7) enters damage delay functions of exponential shape as in [17]. In the adobe delta damage model, given a time τ of the generic loading history evaluated in N points by the Newton-Raphson solver, non dimensional delta functions are introduced according to a principle of decomposition of the Dirichlet boundary condition [13]:

$$\delta D^\tau_{c,t} = D^\tau_{c,t} - D^{\tau-1}_{c,t} = \frac{\Delta_{c,t}}{N}(1 - e^{-(d^\tau_{c,t} - D^{\tau-1}_{c,t})}) \tag{8}$$

where Δ is a non dimensional parameter that bounds the maximum damage rate [13]. The final value of damage at each time step results from the combination of the values in compression and tension [5]:

$$D = 1 - (1 - D_c)(1 - D_t) \tag{9}$$

In the dynamic problem, a consistent mass matrix has been implemented in the equilibrium equation of the finite element model. Time integration of the field equations has been done using the implicit Newmark unconditionally stable scheme [25]. The set of governing equations is integrated within an implicit Newton-Raphson solver. The code has been developed in a C++ environment [26, 27].

3. Mesh sensitivity study in dynamics

The capability of the model to perform mesh objective analyses in statics was demonstrated in [13]. This section analyses its regularization properties in dynamics. To this end, a classical test from literature used to diagnose mesh dependence is adopted [28]. This is the cantilever bar uniaxially loaded in compression [11]. A piecewise velocity profile is commonly applied at the free edge of a 100mm long bar fixed at the bottom (Figure 1). The same analysis is performed for different levels of spatial discretizations [29]. The mesh of the bar is progressively refined starting from a coarse mesh of 10 elements up to 160 elements. Results from numerical analyses are used to verify the local damage distribution and the global reaction force for different levels of mesh refinement.

3.1. ***Quasi static regime***

Prior to the dynamic analysis, the results of a test using the model are compared with the static counterpart to verify the correctness of software implementation in dynamics. The analysis is carried out at a low deformation rate (v=1mm/min) which implies a negligible contribution of inertia in the dynamic equilibrium equation. The following set of elastic and inelastic material parameters of the model are used: E=200 MPa, ν =0.0, ρ=1400 $\frac{kg}{m^3}$, k_{0_c}=$1e^{-3}$, a_c=1000, Δ_c = 10, while t_0=0 s and N=2000. Values are valid for both tension and compression [15]. Results are evaluated with the static analysis in terms of force displacement and damage evolution profile. Considering natural oscillations inherently present in dynamic simulations, the analyses provide the same results (Figure 2a). Furthermore, mesh objectivity is verified in terms of reaction force plots and damage profiles resulting from dynamic equilibrium equations. The model provides the same results independently of the adopted time and spatial discretizations and the damage profiles are consistent along the process of failure (Figure 2b).

3.2. ***Wave propagation problem***

To verify mesh objectivity of the model for a wave propagation problem, sensitivity tests are performed in the case of a significant inertia contribution in the dynamic equilibrium equations. The numerical setup introduced by Sluys in 1992 is adopted [11]. A constant value for the velocity v calculated as $\frac{\kappa f_b}{C\rho}$ (with f_b, C respectively the uniaxial strength and longitudinal wave speed determined by the elastic property of the model and κ a parameter lower than 1) is instantaneously applied (t_o = 0 s) to generate a block wave pulse along the bar which guarantees a linear elastic response of the bar until the loading wave reaches the bottom boundary. The doubling of the stress after reflection assures immediate damage at the boundary and localization of intense straining emerges [10]. The same set of values used in Par. 3.1 for the rate independent parameters of the model is applied. In order to force localization for the fast loading scenario, the parameter Δ in the damage delay formulation is magnified with a factor 500. The adopted time step is $2e^{-6}$s, calculated approximately as

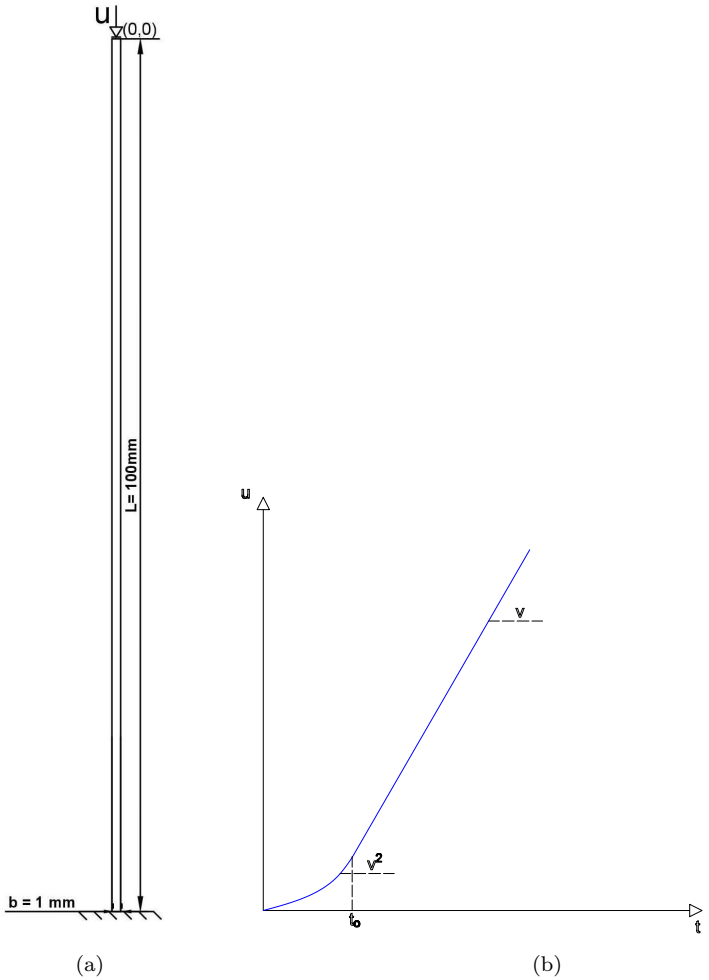

(a) (b)

Figure 1: Numerical setup for the mesh sensitivity study on a uniaxially loaded cantilever bar: geometry (a) and boundary conditions (b)

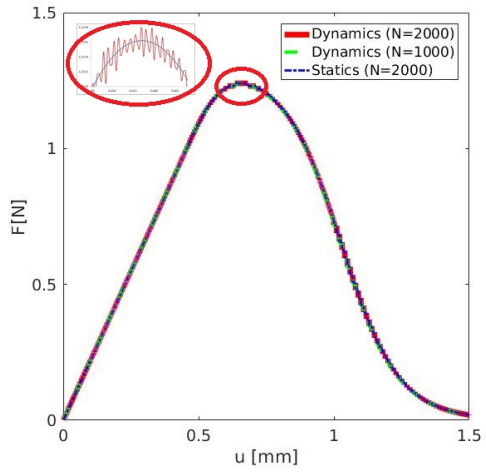

(a)

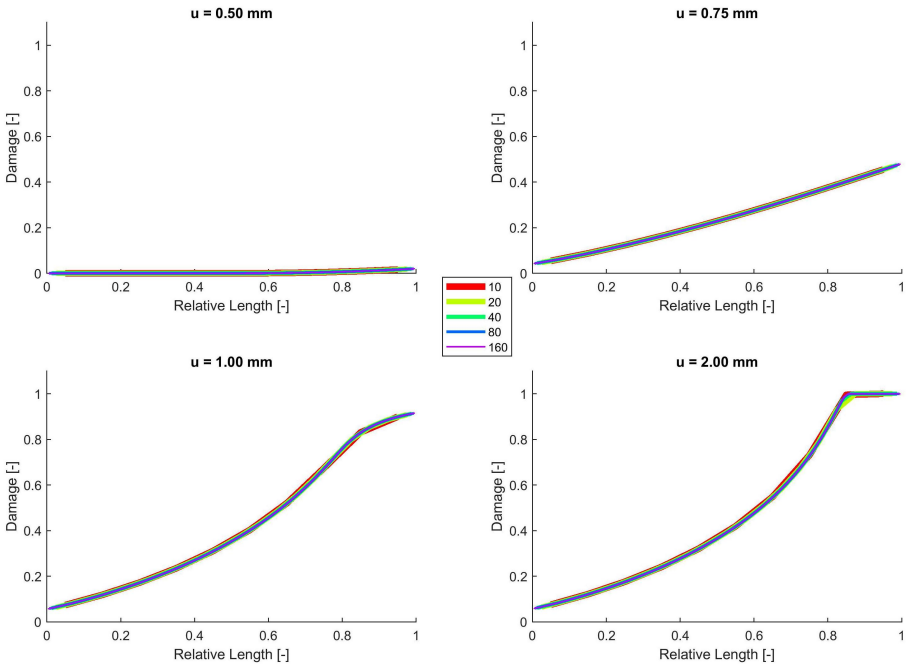

(b)

Figure 2: Force displacements plots (with zoom on peak reaction region) (a) and damage profile extensions along the bar at different stages of simulation (b) for static and quasi static simulations at different temporal (N:1000-2000) and spatial (mesh elements along the bar: 10-160) discretizations (relative length expressed as ratio of the longitudinal coordinate x over the total length L)

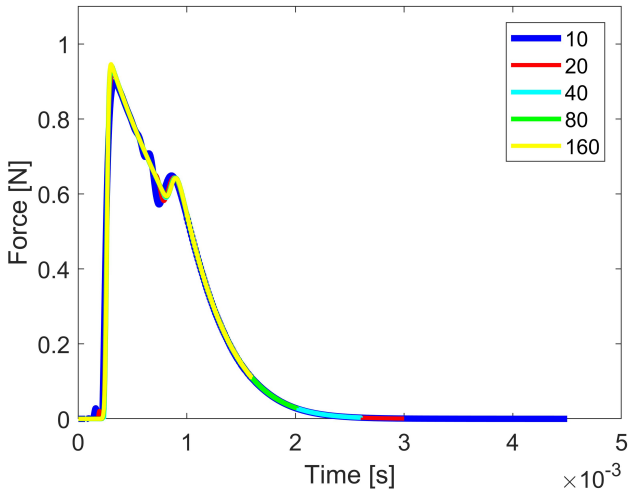

Figure 3: Time history reaction plots at the bottom boundary of a cantilever bar dynamically loaded by a shock wave for different meshes (mesh elements along the bar: 10-160)

1% of the ratio between the length of the bar and the speed of sound C, which is about 400 m/s for the assumed set of elastic parameters [30].

Time history of the reaction force at the bottom boundary nearly overlap for all mesh refinements (Figure 3). Maximum errors in peak load values and toughness of the stress strain curve are always lower than 2%. Damage profiles are consistent for all meshes during the entire simulation (Figure 4).

Results of wave propagation sensitivity test yields the conclusion that the model produces objective simulations in dynamics.

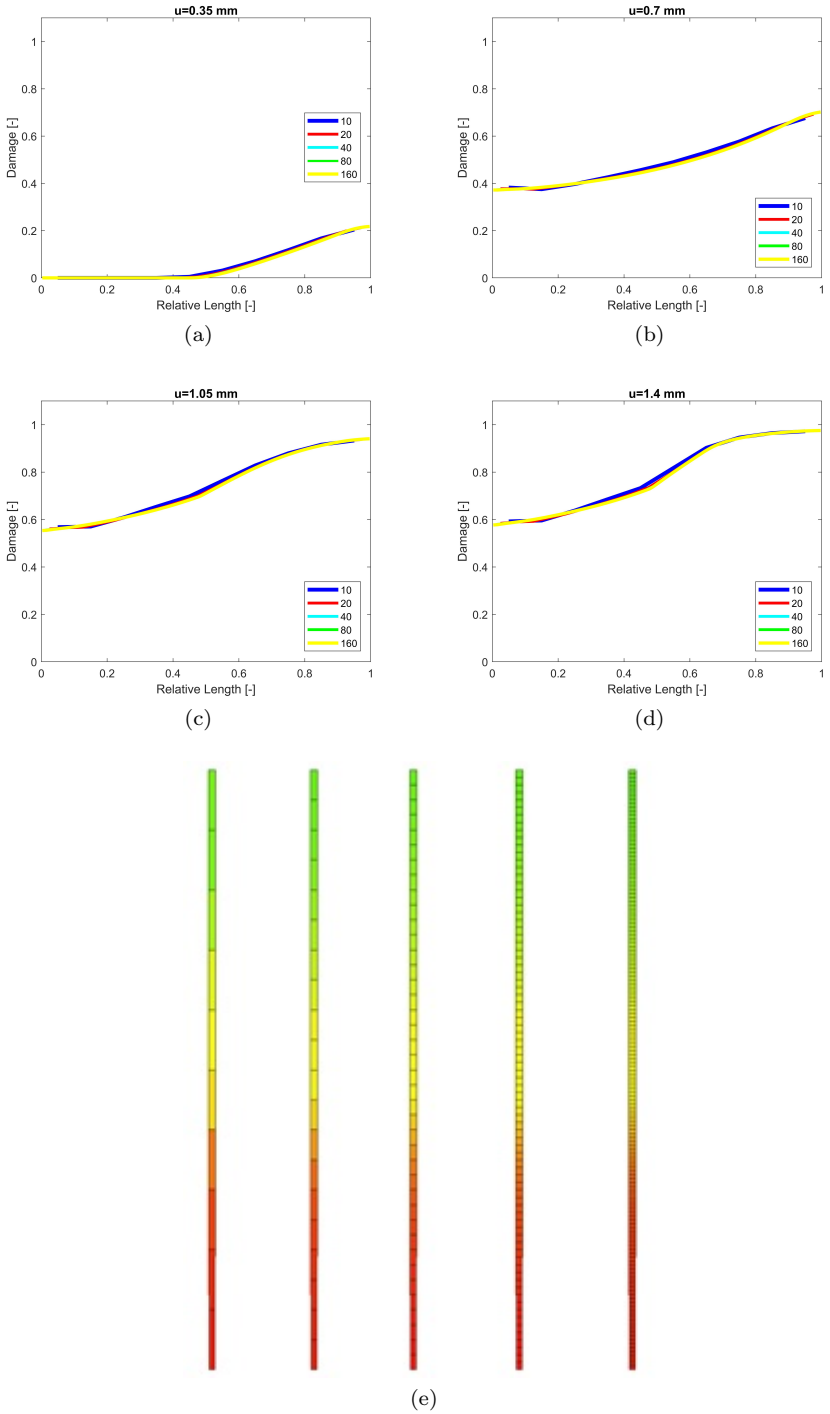

Figure 4: Comparison of damage profile evolutions in the bar at different stages of simulation (a-d) and extension of damage in the bar at time t = $1.8e^{-3}$s (b) for the shock wave propagation test for different meshes

4. A physical interpretation of the model for softening materials

In the previous section the performance of the model in dynamics in terms of mesh independence has been verified. In this section, the original formulation of the delay function is modified according to eq. 10:

$$\delta D^{\tau} = \frac{\Delta\mu(\dot{\epsilon_s}^{\tau})}{N} \ (1 - e^{-\beta(d^{\tau})(d^{\tau} - D^{\tau-1})}) \tag{10}$$

where μ is a function of the loading rate and β a function of the local damage d. The new inclusions are meant to improve the numerical performance of the original formulation by enhancing its consistency with the physics of the material in dynamics.

An extra dependence in the delay function on the value of the local damage d at a given time τ is aimed at enhancing the flexibility of the model to track different shapes of the softening behaviour for various masonry materials. A function μ is introduced to control the maximum damage rate for high loading rates and it allows to use the same model to simulate the material response tested at different deformation rates. In the following two paragraphs, the two enrichments are interpreted in the light of the current knowledge on the mechanical behaviour of quasi brittle materials, using principles of fracture mechanics as well as experimental evidence. Physical consistency and mesh objectivity are firstly numerically tested using the same uniaxial compression test setup shown in Sec. 3 (Figure 1), with loading profiles at the upper boundary of the quasi static regime (1-5 mm/s). Next, modifications are validated against real dynamic tests recently performed by the authors on various soil based masonry materials [16]. Numerical simulations of experimental tests using eq. 10 will be compared and interpreted against the ones obtained using the original formulation in eq. 8. Simulated uniaxial tests consist of dynamic impacts at velocities ranging from 80 mm/s to 4000 mm/s on small cylindrical samples of only clay baked and air dried fibrous adobe materials.

4.1. ***Nucleation time in quasi brittle materials and the numerical delay for ductile curves of response***

A sample of a generic masonry material subjected to an external load in compression does not instantaneously fail due to the formation of the first (micro)-crack. Inside the sample, micro-flaws and defects coalesce and grow until bridging in the macro-crack leads to failure [31]. Thus, a variation in the external load does not result in an immediate effective damage increase and reduction in the bearing capacity of the specimen. There is always a certain *nucleation time* inherent to micro-crack bridging processes.

The delay function of exponential shape in eq. 10 numerically includes this physical property: damage variation due to a variation in the equilibrium equation of forces at the boundary is not instantaneous but delayed [17].

In quasi brittle materials, spatial and temporal progression of micro-cracking processes from the first flaws is found to be dependent on the intrinsic properties of the material and on the external load applied [32, 33].

It is experimentally observed that the nucleation time leading to the bridging process for adobe as well as for other masonry materials is significantly influenced by the external rate [16]. In statics, if propagating flaws encounter stiffer areas, they have the time to deviate around these zones, bridging into macro-cracks, and fracture along a crack path with minimum energy demand is followed. Instead in dynamics, loadings characterized by short time duration and high supply rates induce a forced crack development inside the material also through its stiffer areas, while stress intensity is reduced by the coalescence of other similar micro-cracks nearby the loaded areas [34]. As a result, higher values for compressive strength and strain at peak are observed in the dynamic response of concrete-like materials [35, 36]. In the original delay formulation of eq.8, the influence of loading history on the nucleation time numerically results from the delay $1 - e^{-(d-D)}$ between d at time τ and D at $\tau - 1$. For increasing velocity profiles on the bar of Figure 1, strength (Figure 5a) and damaged profiles (Figure 5b) using the original model and set of parameters as in par. 3.1.1. progressively increase.

However, in [13] a limitation of the original function was observed in correctly capturing the ductile response of masonry bricks and mortar in softening after strength attainment. This will be also shown in Par. 4.1.1 for dynamic loading. This particularly occurs when simulating traditional materials like adobe. These are characterized by a non linear response along the entire deformation process and often denoted by a more ductile softening slope corresponding to a distributed failure due to fiber inclusions. These process could not be fully addressed in [13] using eq.8 and the available set of functions and parameters. The experimental-numerical discrepancy was attributed to a more distributed failure pattern in tests caused by the development of extensive micro cracking during advanced stages of deformation. The influence of the micro-flaws developing along the entire deformation process is mathematically translated in the variable β of the new eq. 10. An increasing brittleness in the response for

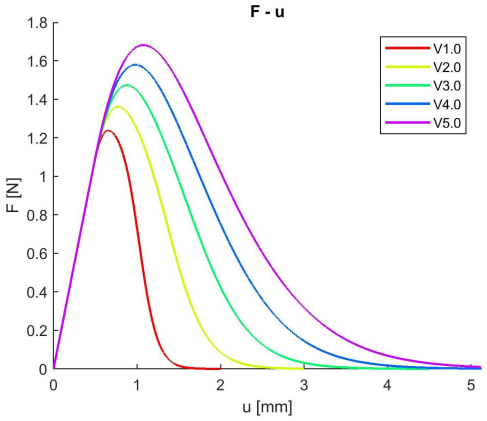

(a)

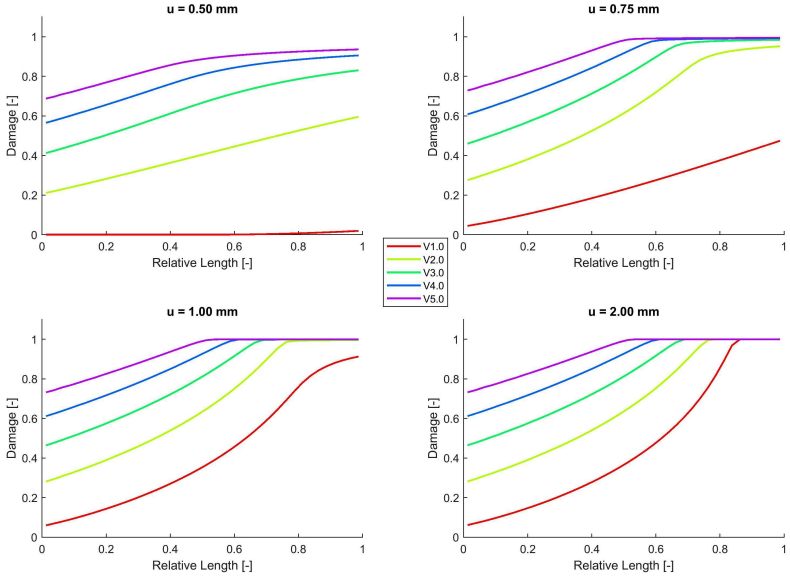

(b)

Figure 5: Force displacement plots (a) and damage profile evolutions (b) in the cantilever bar for dynamic analyses at velocities from 1 mm/s to 5 mm/s using the delay formulation of eq. 8 and parameters in Par. 3.1

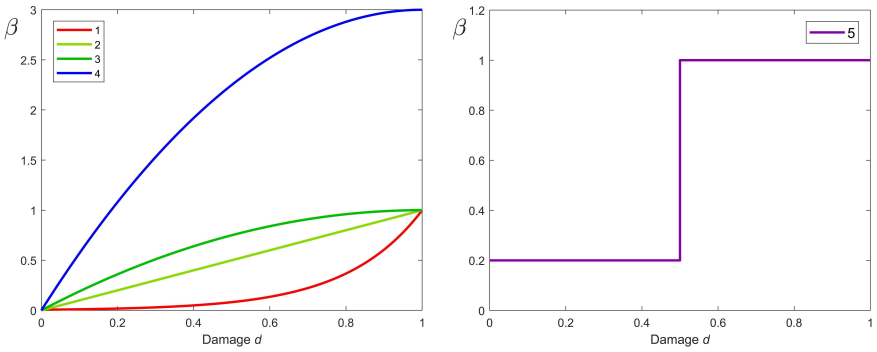

(a) (b)

Figure 6: Different functions for β: continuous (β_{1-4}) and Heaviside function (β_5)

higher values of the parameters ahead of the exponent of the delay function was already observed [9]. However, besides a decay of the strength, the shape of the resulting softening slope remain the same using constant parameters. Instead, the mineralogical properties and inter-particle interactions influence the micro-flaws size and distribution which dictate the speed and progression of the micro-cracks coalescing into the structural macro-crack up to failure [16, 33]. As a result, the softening slope can be significantly different between different materials and change during the deformation process according to the mineralogical properties of the mixture. The effects of these properties on material failure are phenomenologically represented in damage models by the parameters of the local damage evolution laws (eq.7). Thus, the dependence of the softening process on the intrinsic mixture properties is represented by a β function in the delay of eq. 10 that governs the actual history of the local damage d along the whole deformation process. This results into a direct dependence of β on the value of the local damage d at time step τ. The entire non linear phase of the material response changes after introducing β, including the initial damage rate and the softening slope evolution. They vary according to the particular function used for the evolution for β. This is shown in the following, using the test of the compressed bar presented in Sec.3. Four different continuous functions of the local damage d presented in eq. 11 are applied for the same model already calibrated in Par. 3.1 (Figure 6a). These are exponential, linear and quadratic functions that represent different gradients at a given value of damage d during loading history.

$$\begin{cases} \beta_1 = e^{5(d-1)} & \\ \beta_2 = d & \beta_5 = 0.2 \ (if \ d \leqslant 0.5) \\ \beta_3 = -d^2 + d & \beta_5 = 1.0 \ if(\ d \geqslant 0.5) \\ \beta_4 = -3d^2 + 6d & \end{cases} \tag{11}$$

According to the different functions and inherent slopes at a given damage d, the

corresponding four curves are characterized by different damage rates, softening branch slopes (Figure 7a) and damage evolutions (Figure 7b). The flexibility of the new formulation is further emphasized using a discontinuous function of d for β. A Heaviside function which presents a sudden jump in the middle of the damage evolution d as in eq. 11 is applied in the model (Figure 6b). This may correspond to a material response characterized by a quasi brittle meso-structure that is dramatically weakened at a certain deformation level. For example, this can result from a change of rate in the micro-cracks bridging processes inside the material due to the specific properties of the mixture. According to the depicted trend, curve 5 in Figure 7 initially shows a significant non linear response and a distributed damage profile, before sudden failure with damage localization and a brittle softening branch after crisis. Choice of the specific relationship for β depends on empirical evidence characterizing material failure in compression both in force-displacement plots and damage patterns.

The enrichment in eq. 10 does not affect the mesh dependence regularization properties of the algorithm for all the proposed functions (Figure 8).

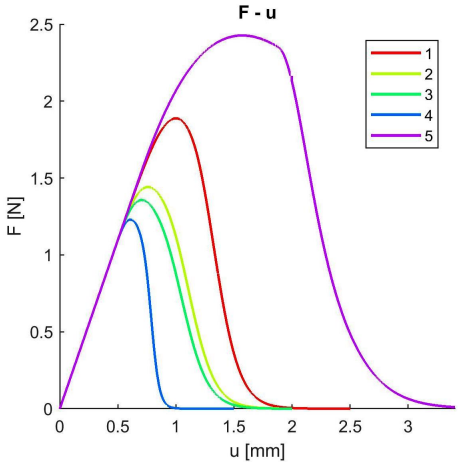

(a)

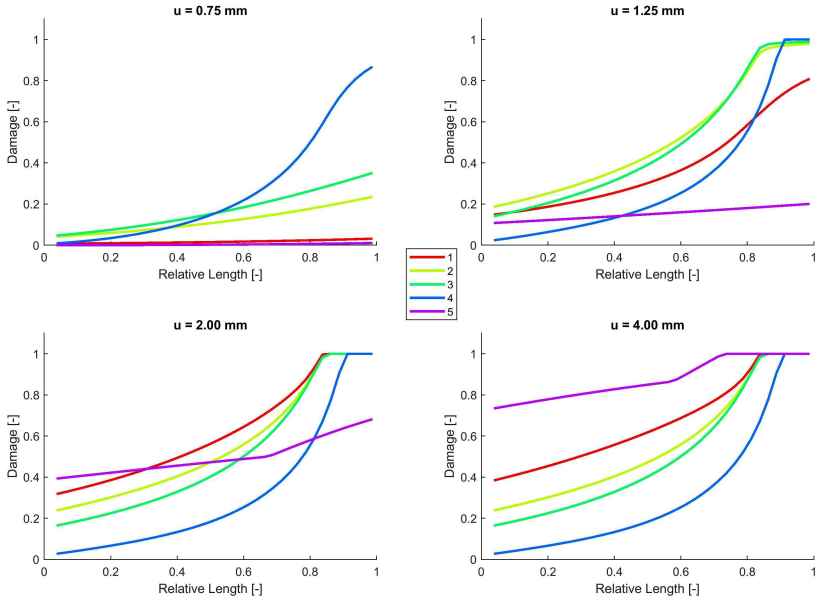

(b)

Figure 7: Force displacement plots (a) and damage profile evolutions (b) for dynamic analyses on the bar loaded at v=1 mm/s using the five functions (β_{1-5}) in eq.11

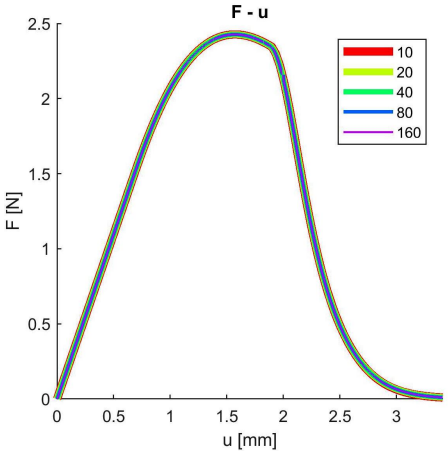

(a)

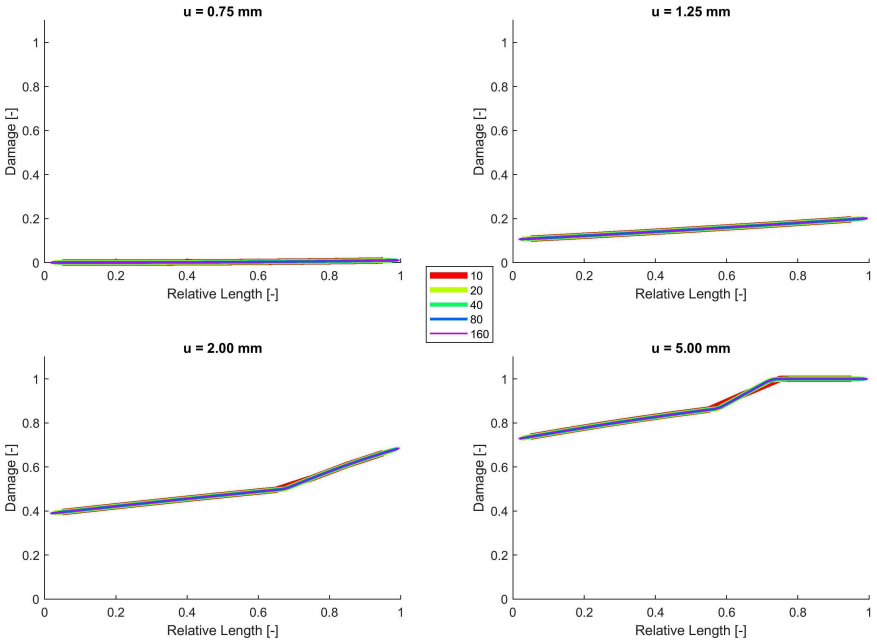

(b)

Figure 8: Force displacement plots (a) and damage profile evolution (b) for different meshes using β_5 (for an applied velocity of 1 mm/s)

4.1.1. ***A numerical application of the new formulation***

Correctly capturing the complete failure in compression is fundamental for non linear analyses of masonry materials [37, 38]. The effect of the new formulation is tested in this paragraph on the simulation of the dynamic failure in compression of masonry components. For this purpose, the dynamic response of adobe is used as an experimental reference. Adobe bricks are commonly constituted by soil mixed with fibers and dried under the sun. As a result, their behaviour in compression is usually characterized by a nonlinear response with ductile softening and a distributed failure pattern that progresses during the entire deformation process, with the development of secondary cracks starting after attainment of the main one.

A joint experimental campaign between Delft University of Technology, TNO, Dutch Ministry of Defence and European Commission performed uniaxial compression tests on adobe samples at high rates of deformations [16]. Cylindrical samples of 40mm in diameter and with unitary slenderness of an adobe brick with 20% by weight of fibers in the soil mixture were subjected to displacement controlled analyses at a constant rate of 90mm/s. The response of the samples was characterized by a more ductile softening slope and a distributed pattern of cracks observed on the entire surface. These usually started before reaching the maximum reaction force. At least two main cracks developing at different moments of the test in softening of whom the first usually starting from one corner of the specimen were observed during testing. A representative test is chosen as the experimental reference.

For numerical simulation purposes, the constant loading profile experimentally applied to the specimen by the displacement driven steel platens is directly extracted from the test and applied at the top of the numerical setup. Boundary conditions are shown in Figure 9. Axial symmetry is implemented in the model to simulate the 3D cylindrical shape of the sample and only half of the brick is simulated and meshed with a 0.5mm element size. Geometrical dimensions of the numerical sample are approximately the same as in experiments.

To enhance consistency in the comparison of the effects of the new formulation, the same set of hypotheses used in [13] to simulate the static tests on adobe are adopted. In the following, only the main ones are recalled:

- For the Young's modulus, the mean values of secant elastic stiffness experimentally derived is used (E=40 MPa). Symmetry in the parameter in tension is assumed. A 0.1 value for the Poisson's ratio is assumed [39]. In addition to the static hypotheses, the average value of density found for adobe from tests (1100 kg/m^3) is used;

- The parameters of the modified Drucker Prager surface of eq.(3) in Par.2 are modified to include an inscribed Drucker-Prager smoothed version of

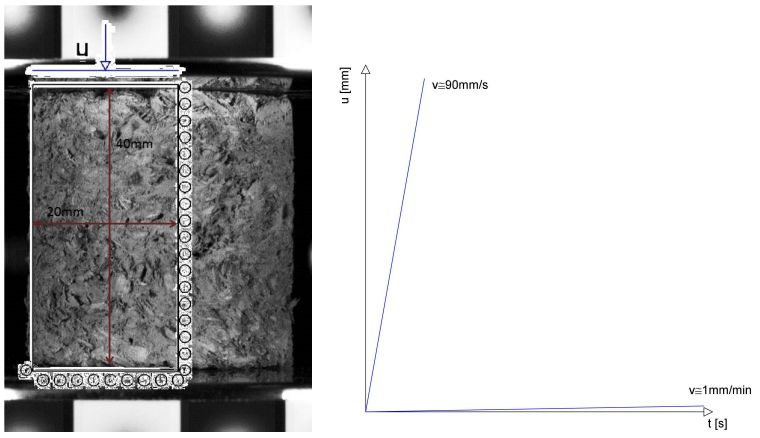

(a) (b)

Figure 9: Shape and geometry of experimental and numerical setup (a), with experimentally derived loading history applied at the top boundary of the numerical sample (b)

Mohr Coloumb failure in compression. The coefficient $c_1 - c_4$ of eq.3 are:

$$\begin{cases} c_1 = \frac{1}{(1-2\nu)} \\ c_2 = \frac{1}{2\sqrt{2}(1+\nu)} \\ c_3 = \frac{tg(\phi)}{(1-2\nu)} \\ c_4 = \frac{\sqrt{3}}{2(1+\nu)} \end{cases} \tag{12}$$

in which the internal friction angle ϕ=15^o is chosen corresponding to organic soil [13].

- For the damage initiation strains in compression, the mean value for the initial deviation from linearity in the stress strain diagrams is used (k_{oc}= 2.5 e^{-2}). Half of this value is taken for the damage initiation strain in tension (k_{ot}= 1.25 e^{-2}).
- A mechanical defect, with damage initiation strain equal to 1 e^{-3}, is imposed at the corner of the specimen.
- The damage evolution laws in eq.(7) are simplified in compression according to a pure exponential law whereas in tension according to the linear softening characterized by a steeper slope (a=0).

As in [13], at first only the two parameters in compression (a, Δ) of the original formulation in eq.8 (β=1) have been calibrated to match the maximum reaction force and the corresponding displacement experimentally derived in the force displacement curve by dynamic testing (a=200, β=1, Δ=350). The best fitting numerical curve and the corresponding failure mode are compared with the response observed in experiment in Figure 10 ("original model"). As in [13],

the numerical plot shows a brittle slope in softening against the more ductile experimental response. Furthermore, the corresponding failure mode is only recalled in the simulation, with a too large width of the primary crack starting from the corner and a more localized damage distribution in the numerical sample.

Next, the dependence of β on d as discussed in Par. 4.1 is fully integrated in the formulation. In order to further test the flexibility of the model after β inclusion, the same simulation is repeated using the set of parameters previously calibrated (a, Δ) and only combined with the new dependency on β. After testing different functions with shapes as in eq.11, a linear function of the type $\beta_2 = (r_1 - r_2)\ d + r_2$ proves to be the best fit, with r constant parameters calibrated as about r_1=0.2 and r_2=1. The resulting curve and the corresponding failure mode are compared again with experiments in Figure 10 ("enriched model").

Despite restrictions in the initial setup and hypotheses, after inclusion of the new function, the model is capable to correctly capture the ductile softening branch of response experimentally observed. Furthermore, given the limitation of deterministic models to correctly capture cracks that in adobe usually start from clay concentrations or fiber-induced areas of de-adherence, the total extension of the numerical damage is larger than before and more consistent with the area of the tested sample interested by cracks. In addition, a localized primary crack starting from the corner followed by a second numerical crack with branching now numerically resembles the progression experimentally observed (Figure 11d).

As a confirmation of the findings in Par. 4.1, the formulation including the new dependency preserves the feature of mesh independence of the original model (Figure 11a-b) along deformation history, including the first stages of the non linear softening, where maximum discontinuity in slope arises with respect to the original curve (Figure 11c-d).

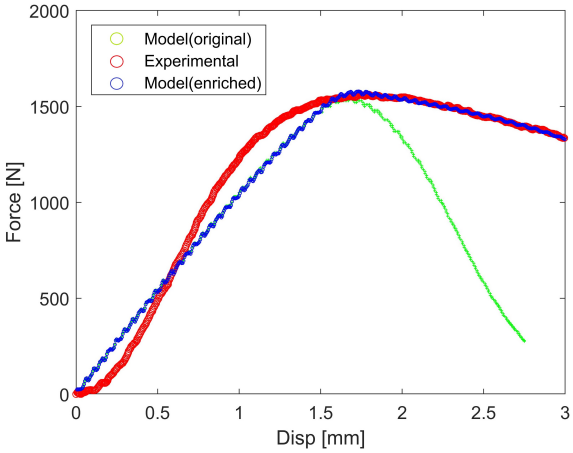

(a)

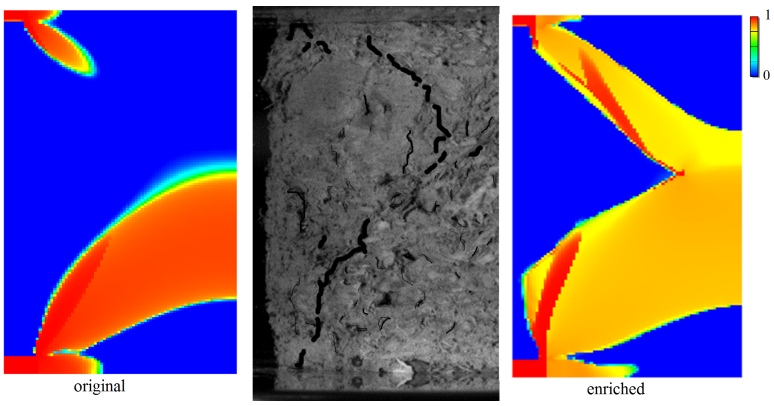

(b)

Figure 10: Numerical comparisons of force displacement curves (a) and cracking patterns at about 3 mm of deformation (b) with experimental compression test on adobe at v = 90 mm/s between the best fit numerical curve using β=1 (original model) and β as a linear relation of damage d (enriched model)

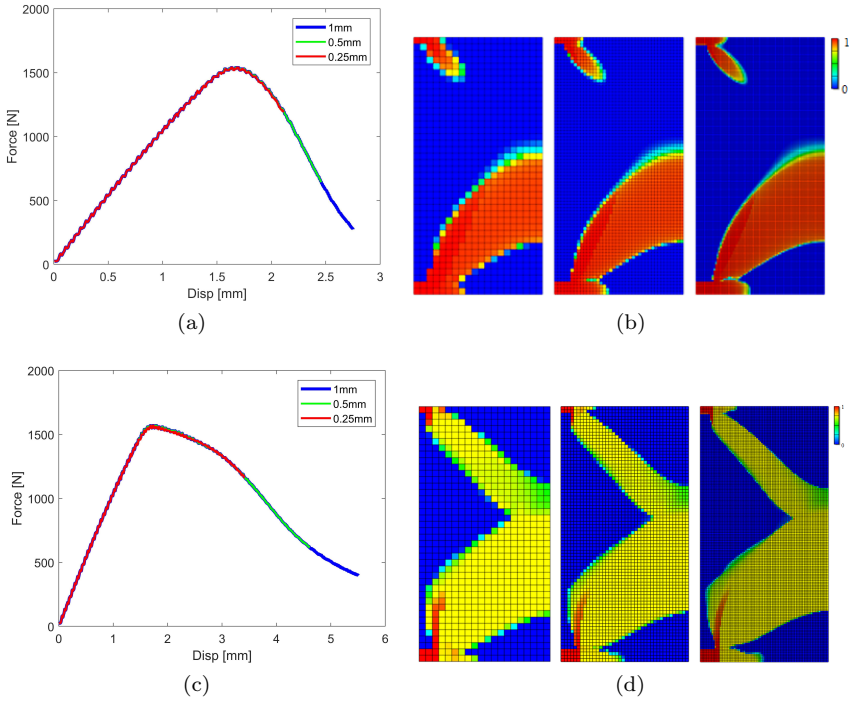

Figure 11: Comparison of numerical force-displacement curves and failure patterns at step i=550 for different meshes using the original model (a-b) and the enriched formulation after β in eq. 10 (c-d)

4.2. Crack propagation velocity in quasi brittle materials and the numerical delay for rate dependent analyses

The amount of delay in the cracking process is numerically scaled by a factor Δ in the adobe delta damage model. For a given loading profile, it mathematically determines the maximum value of damage rate [40]. In the early nineties, bounded models introduced a cap to damage dependent models ($\dot{\tau_c}$ in the original formulation in [41]). This is consistent with assuming a maximum velocity to flaws propagation. In quasi brittle materials, many micro-cracks coalesce propagating through the specimen into a dominant macro-crack at a certain speed and orientation according to the mineralogical composition of the material meso-structure [32]. Thus, it is common practice in literature to attribute a constant value to the numerical parameters that define the maximum failure rate, usually calibrated in single tests of the dynamic regime [42, 24]. However, this property is not solely determined by the mineralogical composition of the material. In quasi-brittle materials, the rate of crack bridging is significantly influenced by temperature, moisture and loading conditions, with the applied loading rate in particular [43, 44]. In this regards, cracks growth rate depends on the supply energy rate and increases with increasing loading rates [45]-[48]. Thus, a maximum damage rate $\dot{D}$ for a given loading velocity applied exists but this numerical property must vary with the loading rate [41, 42]. This feature is now integrated in the delay formulation of eq. 10 introducing a direct dependence between Δ and a function μ of the applied strain rate. In fact, assuming a constant value for the Δ parameter as in eq. 8 results in an unrealistic sensitivity of the model when higher loading rates are applied. This is shown analysing the response of the compressed bar in Par. 3.1.1. and loaded at increasing applied velocities, from a quasi static constant rate (v_1=1mm/s) to one and two higher orders of magnitude (v_2=10 mm/s, v_3=100mm/s). Using the original formulation of eq. 8 (μ_0 in eq. 13) on the model calibrated in Par. 3.1.1, numerical simulations show a high sensitivity in the response to higher loading regimes (Figure 13a). In particular, a dynamic increase factor (or *DIF*, the ratio of the dynamic value of a property with respect to its static one) in strength of about 10 is achieved for a jump of two orders of magnitude in the maximum velocity applied at the boundary of the bar (Table 1). Instead, experimental values of the increment of strength in dynamics for the same dynamic ranges are usually lower than 3 for quasi brittle materials [49].

Dependence of Δ on the loading rate is incorporated in the numerics of the model introducing a function μ of the slope of the Dirichlet boundary condition applied at each time step. Average strain rates are then determined according to the selected geometry and loading direction. Three different continuous functions reported in eq. 13 have been tested. As in the numerical test of Par. 4.1, examples of linear, quadratic and square functions address different slopes in the μ function at a given time and thus provide different viscous contributions

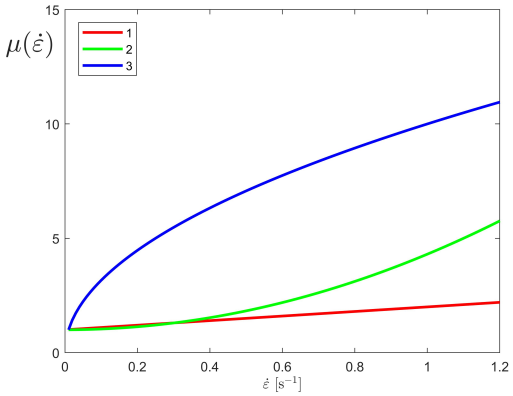

Figure 12: Slope of the different rate dependent functions μ_{1-3} in eq. 13

to Δ (Figure 12).

$$\begin{cases} \mu_0 = 1 \\ \mu_1 = 10^{-3}\dot{\epsilon}_s + 1 \\ \mu_2 = 3\dot{\epsilon}_s^2 \\ \mu_3 = 10\sqrt{\dot{\epsilon}_s} \end{cases} \tag{13}$$

The sensitivity to rate inherent to the original model (μ_0) for all the material properties is significantly restrained at high strain rates by using the functions μ_{1-3} in eq.10 (Figure 13b). Dynamic increase factor values at both velocities applied become closer to experimental results usually associated to quasi brittle materials dynamically loaded [49]. This new dependence in the model induces a specific material sensitivity to rate in the slope of the force displacement curves of the bar loaded at increasing velocities according to the particular function used for μ (Figure 13c-e). Thus, the dynamic increase factors in strength and deformation differently vary in dynamics according to the influence that the slope of the function μ exerts on damage localization determined by the maximum damage rate at a given strain rate (Table 1). Among the tested functions, μ_3 results in the largest restrain of the enhancement of the dynamic material properties.

Also in this case, the new dependence does not alter the regularization properties of the model for any of the functions tested in eq. 13 and applied velocities (Figure 14).

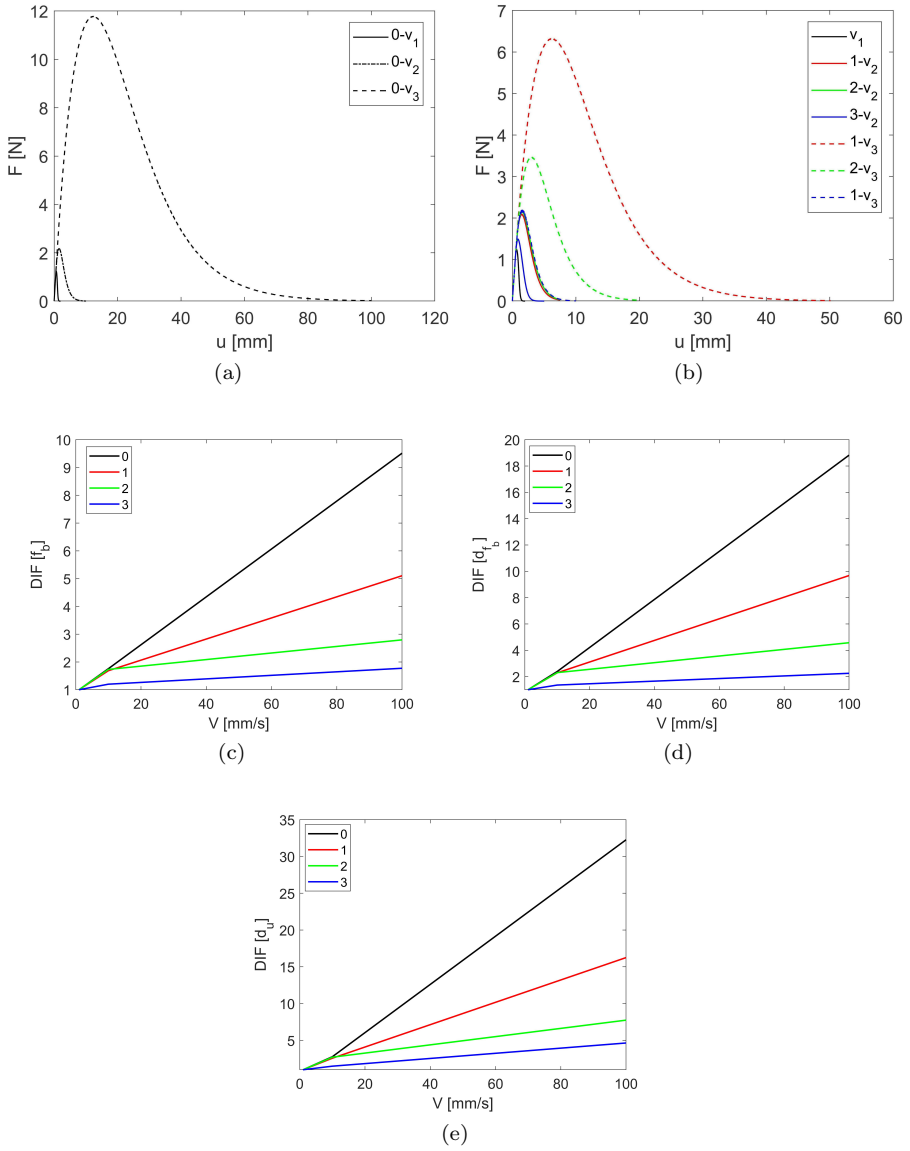

Figure 13: Force-displacement curves for the cantilever bar loaded in compression at velocity v_1=1 mm/s, v_2=10 mm/s and v_3=100mm/s using the original model (a) and the three functions μ_{1-3} in eq. 13 (b), with corresponding plots of the dynamic increase factors in strength (c), displacement at peak load (d) and ultimate displacement (e) based on linear interpolation

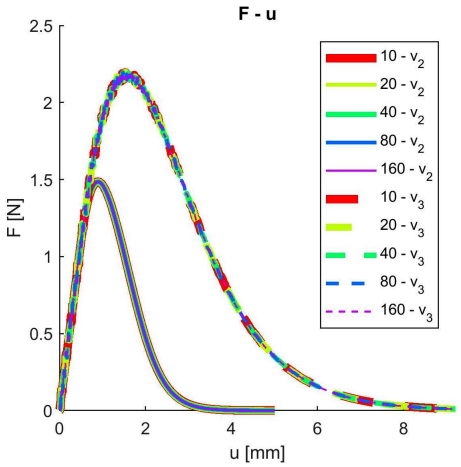

(a)

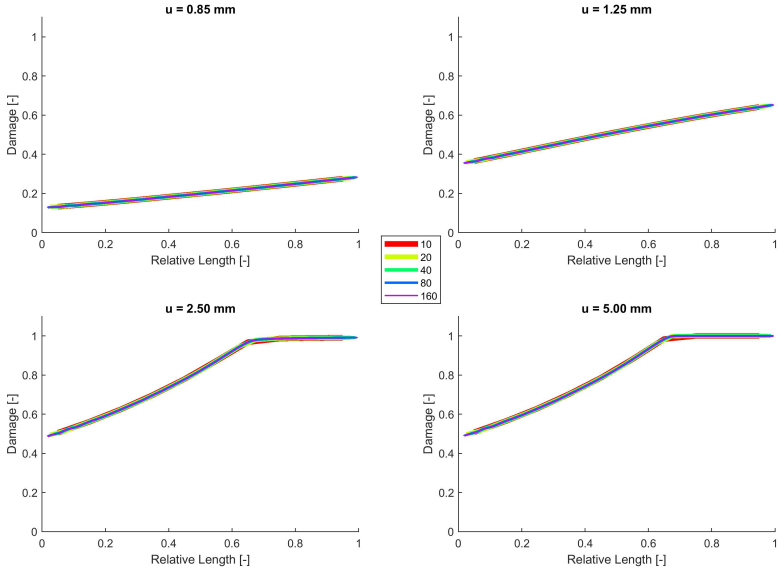

(b)

Figure 14: Comparison of force displacement curves (a) and damage profile evolutions (v_2) (b) for four mesh refinements (10-160 elements) of the bar dynamically loaded using μ_3

Table 1: Dynamic increase factors values for compressive strength, displacement at peak load and ultimate displacement in softening after 20 % of strength decay for velocity profiles v_2 and v_3 on the bar using μ_{0-3} in eq. 13

	DIF_{f_b}		$DIF_{d_{f_b}}$		DIF_{d_u}	
v	*2*	*3*	*2*	*3*	*2*	*3*
μ_0	1.76	9.52	2.39	18.83	2.77	32.27
μ_1	1.69	5.10	2.29	9.68	2.59	16.25
μ_2	1.73	2.80	2.30	4.57	2.71	7.74
μ_3	1.20	1.77	1.36	2.25	1.49	4.64

4.2.1. ***A numerical application of the new formulation***

Correctly addressing the rate of increment of the material strength in dynamics (DIF) is of paramount importance for engineering design of masonry against highly dynamic loadings [50]. Compression tests on modern geomaterials in literature always indicate a certain increment in the unconfined compressive strength of the material in the dynamic regime, included between 1.5 and 3 times the static strength for high strain rates loadings [36]. Strength increment rates for quasi brittle materials are currently hypothesized mainly using analytical formulations developed empirically from tests on modern cementitious materials with different properties and compositions than traditional bricks [49]. Many concrete modellers use the widely accepted standard reference for concrete by Committee Euro-International du Beton (CEB) [51]. The CEB recommends the strain rate induced strength increment formulation for normal concrete as:

$$\begin{cases} DIF = (\frac{\dot{\epsilon}}{\dot{\epsilon_s}})^{(1.026\alpha)} for\ \dot{\epsilon} \leqslant 30s^{-1} \\ DIF = \gamma(\frac{\dot{\epsilon}}{\dot{\epsilon_s}})^{(0.33)} for\ \dot{\epsilon} \geqslant 30s^{-1} \end{cases} \tag{14}$$

where $\dot{\epsilon}$ is the current strain rate in dynamics, $\dot{\epsilon}_s$ is the reference static strain rate (equal to 3 10^{-5}) and:

$$\begin{cases} \alpha = \frac{1}{5+9(\frac{f_b}{f_{bo}})} \\ \gamma = 10^{6.156\alpha-2} \end{cases} \tag{15}$$

where f_{bo} is a reference strength of 10 MPa. Instead, only few numerical applications aimed at simulating the dynamic increment of the mechanical performance of materials can be found in literature [52].

The capability of the new delta formulation to limit the rate sensitivity in dynamics of the original model and correctly addressing the rates of increment in strength experimentally associated to masonry materials at higher strain rates is validated in this paragraph. The effect of the new formulation for Δ in eq. 10 in the model is tested on the numerical simulation of the dynamic increase factors in strength at different dynamic rates experimentally derived for clay masonry bricks. To this end, the results of an experimental campaign recently performed by the authors is chosen as a reference [16]. This was aimed to analyse the rate of enhancement of the maximum strength exhibited by cylindrical soil samples baked in the oven and subjected to uniaxial compression tests at three sequent orders of strain rates, from statics to high velocity impacts. Strain rates of the order of 120 s^{-1} were achieved using a Hopkinson bar. Thus, cylindrical samples with same geometry as in Sec 4.1.2 were uniaxially compressed at constant rates of respectively 1 mm/min, 90 mm/s and 4200 mm/s. As a result of the experimental campaign, a normalized strength of 2.5 MPa was derived in statics averaging the peak reactions over the cross section areas. The average dynamic increase factors in strength were consequently calculated after dynamic testing as circa 1.3 times the static value for strain rates of 3 s^{-1} and 1.8 for strain rates of 120 s^{-1}. The experimental dynamic increase factors for the tested bricks lie on the lower region of the cloud of data commonly associated to the dynamic

performance of concrete. Therefore, models commonly used to design concrete in dynamics like the CEB model in eq.14 only hardly address the dynamic trend associated experimentally to clay bricks (Figure 16a).

Next, the numerical model is used to predict the variation in normalized strength experimentally observed for clay at all the different rates. A proper assessment of the true material properties from experimental test data at high rates requires the evaluation of the contribution of radial inertia and platens-specimen friction on the dynamic strength enhancement. However, this paragraph is limited to reveal the functionality of the implemented feature of μ in the delay function against experimental trends recently found. Therefore, the effects of friction or inertia on the experimental results are not quantitatively included in the numerical discussion.

Static tests using the model are performed on the setup of Figure 9. Similarly to the set of hypotheses described in Par.4.2.1, the elastic properties of the model are taken from the average values experimentally derived in statics for the clay bricks (ρ=1800; ν=0.1; $k_{0_{c,t}}$=0.6 e^{-2} and E= 140 MPa). Also as in Par. 4.1.2, the parameters of the original delay of eq. 8 in Sec.2 are calibrated to address the mean force and displacement coordinates corresponding to the maximum reaction force experimentally derived in the static test (a=108;Δ=6.0). As a result, the first point of the DIF plot numerically determined for the static regime in the graph of Figure 16b (DIF=1) coincides with the experimental value.

Using the set of parameters calibrated in statics, the model is used to perform numerical simulations in the dynamic regime at the two different loading rates. For this purpose, the average displacements histories are directly extracted from the laboratory tests at both rates and applied on the model with same geometry as in tests. For the intermediate loading regime corresponding to an applied displacement rate of v = 90mm/s, the same setup shown in Figure 9 and used in Par. 4.1.2 is herein applied for simulations purposes. In the case of high strain rate tests using the Hopkinson bar, the deformation rates extracted from the reflected and transmitted waves experimentally derived as functions of time are directly applied to the numerical setup of Figure 15.

Firstly, dynamic simulations are performed using the original model calibrated in statics with a constant μ_0=1 ("original model"). The values of normalized strength in compression are numerically derived from both tests and correspondingly plotted as dynamic increase factors in Figure 16 together with the experimental values in [16]. Numerical simulations using the original model clearly show an unrealistic over-estimation of the compressive strength of the brick for the considered range of strain rates in dynamics (Figure 16b). Next, the dependence of Δ on the rate $\dot{\epsilon}$ via the function μ in eq. 10 is integrated in the model ("enriched model"). The same dynamic analyses are thus repeated using different shapes for μ as in Figure 12. A linear dependence for μ=2($\dot{\epsilon}$+1) proved to be the best fit.

The normalized compressive strengths numerically derived from the reaction plots of both tests are plotted again as dynamic increase factors of the static strength in Figure 17 and compared with the experimental values. The model is

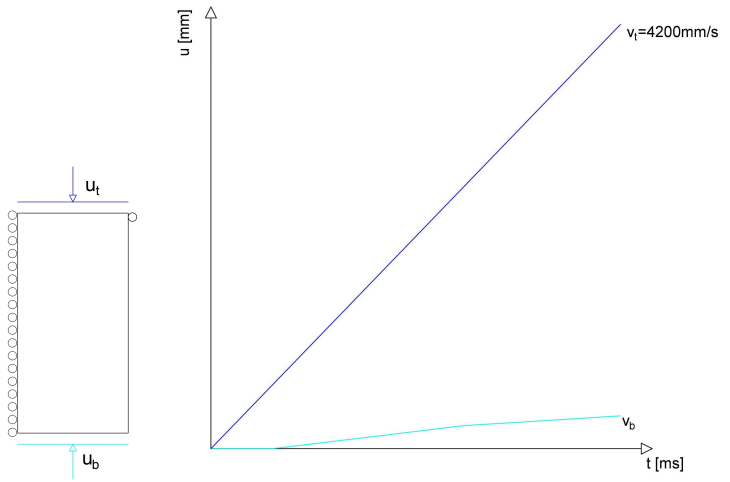

Figure 15: Numerical setup used for the simulation of the Hopkinson bar tests in [16] (a), with applied loading histories at the boundaries of the numerical sample derived directly from experiments (b)

now capable to correctly quantify the experimental strengths of the tested bricks with a good approximation at all loading rates, including above 100 s^{-1}, where standard are found to overestimate the experimental data [53]. Obtaining full consistency with the experimental stress-strain curves goes beyond the specific goal of the current simulations. However, the numerical plots already lie within the experimental envelopes of the material for the two dynamic regimes and the numerical assessment of the average critical time t at which the maximum strength arises is close to the experimental results at both rates (Figure 17). As for Par. 4.1.2, the formulation including the new dependence preserves the feature of mesh independence of the original model and refining the mesh the dynamic increase factors do not change at the intermediate (DIF≈1.3) and high (DIF≈1.8) rates (Figure 17).

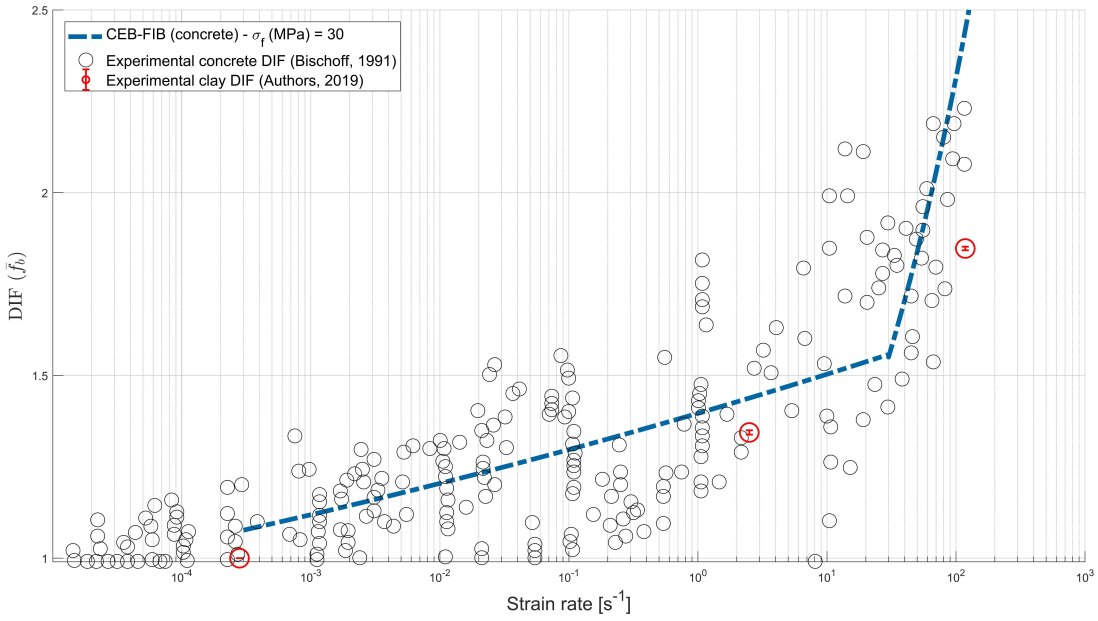

(a)

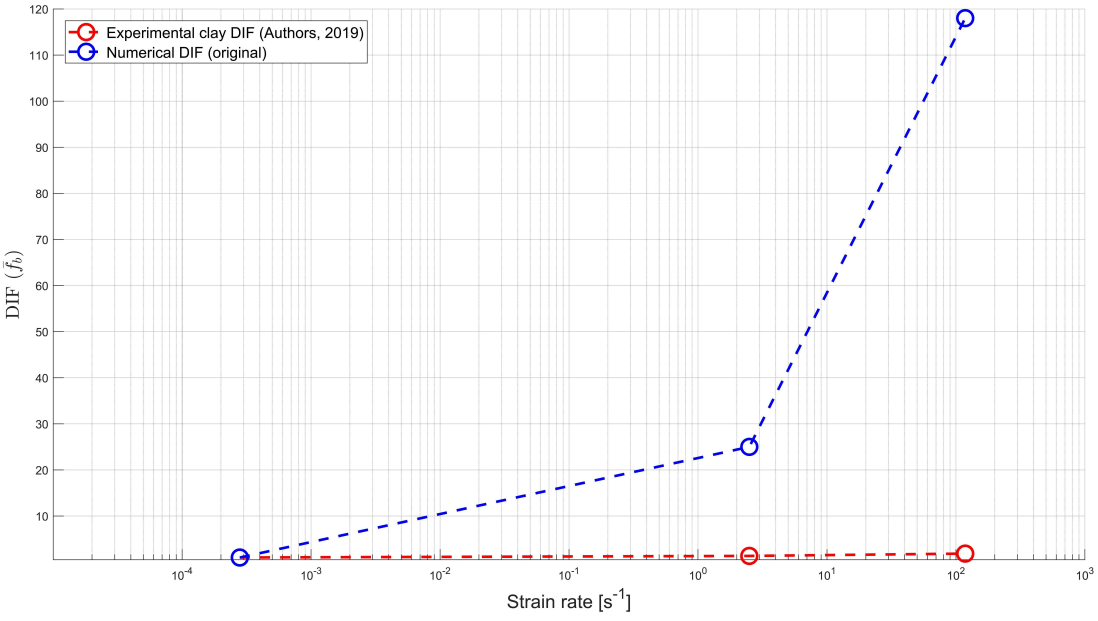

(b)

Figure 16: Experimental dynamic increase factors in strength for the clay based bricks tested by the authors (in red), with respect to experimental data usually associated to concrete at the same strain rates (in black) and CEB-FIB predictive model for high strain rate loadings (in blue) (a); Experimental-numerical comparison of the dynamic increase factor function using the original numerical model (b)

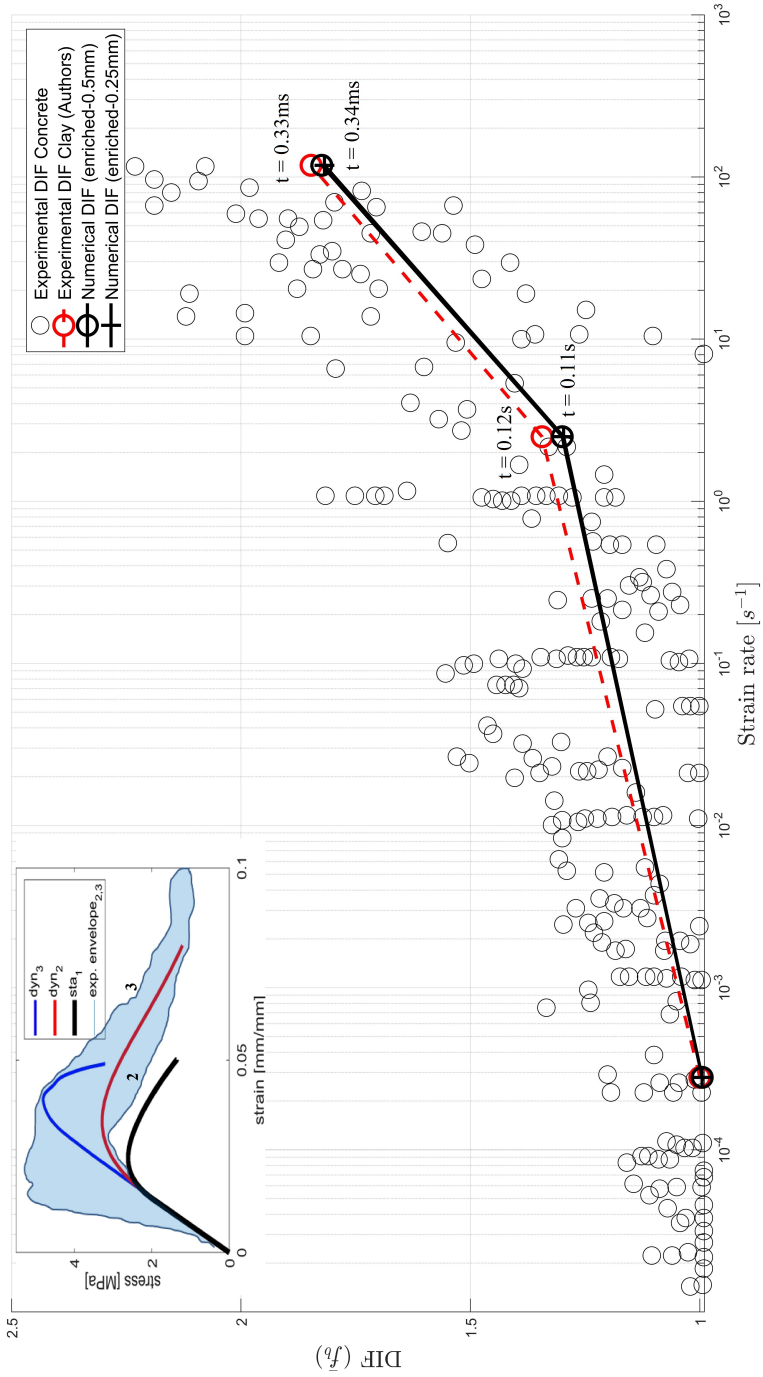

Figure 17: Experimental-numerical comparison of the dynamic increase factor functions in strength and of the critical time (t) at strength attainment using the enriched numerical model (with μ in eq. 10) for two different mesh refinements, with examples of numerical stress strain curves within the experimental envelope for the two dynamic rates

5. Conclusions

In this study, the proper regularization properties of a local rate dependent damage model have been demonstrated in dynamics. Furthermore, the formulation of the original regularization algorithm has been improved in order to address the behavior of quasi brittle materials used in masonry for a wide range of strain rates, from statics to the ones corresponding to earthquakes up to high velocity impact.

The original model had a limited capability in addressing failure of ductile materials characterized by mild softening and distributed damage. In this study, the original damage delay model has been enriched by a direct dependence on the actual local state of damage. This physically refers to the influence that the mineralogical properties of the meso structure of a material exerts on the coalescence and propagation of micro-flaws during the entire deformation process. As a result, the model has gained flexibility in the capability of correctly addressing the dynamic response in compression of various materials, also when characterized by ductile failure.

Furthermore, the response of the original model in compression showed an extreme sensitivity to the applied loading rate when the maximum damage rate of delay is a constant and calibrated with respect to only one loading condition. As a result, the dynamic increase factors for the main mechanical parameters were not consistent with experimental data for most building materials in dynamic compression tests. In this study, the original damage delay formulation has been enriched by a direct dependence on the actual applied loading rate. This physically refers to the viscous influence that deformation rate exerts on the damage progress and maximum crack velocity in the material. As a result, the model is capable of describing the rate dependence exhibited by masonry materials in dynamics, including the assessment of dynamic increase factor functions.

The choice of the shape and of the parameters values of the functions to be used for β and μ can be derived directly from mechanical tests on samples and thus they phenomenologically address the effect that the specific mineralogical properties, inertia and viscosity at a micro-scale exert on the material failure at a macro-scale in statics as well as in dynamics.

Acknowledgement

MSc candidate T. Martin Tran is acknowledged for the simulations of this paper performed during his MSc thesis project.

References

[1] T. Li Piani, Operative Guidelines for Protection of Places of Worship: A new approach toward security design of sensitive buildings, Institute for Advanced Strategic and Political Studies, ISBN:97888940373-2-6, Milan, 2017.

[2] L. Pereira, New computational approach towards the simulation of concrete structures under impulsive loading, Ph.D. thesis, Delft University of Technology (TU Delft) (2018).

[3] J. Mazars, F. Hamon, S. Grange, A new 3D damage model for concrete under monotonic, cyclic and dynamic loadings, Materials and Structures (2015) 3779–3793doi:10.1617/s11527-014-0439-8.
URL http://link.springer.com/10.1617/s11527-014-0439-8

[4] P. Forquin, Brittle materials at high-loading rates: An open area of research, Philosophical Transactions of the Royal Society A: Mathematical, Physical and Engineering Sciences 375 (2085) (2017). doi:10.1098/rsta.2016.0436.

[5] L. F. Pereira, J. Weerheijm, L. J. Sluys, A new effective rate dependent damage model for dynamic tensile failure of concrete, Engineering Fracture Mechanics 176 (2017) 281–299. doi:10.1016/j.engfracmech.2017.03.048.
URL http://linkinghub.elsevier.com/retrieve/pii/S001379441630474X

[6] M. Jirasek, Z. Bazant, Model for Localization of Softening and Size Effect, in: Inelastic Analysis of Structures, 2002, Ch. 26.

[7] F. van der Meer, L. J. Sluys, Continuum Models for the Analysis of Progressive Failure in Composite Laminates, Journal of Composite Materials 43 (20) (2009) 2131–2156. doi:10.1177/0021998309343054.
URL http://jcm.sagepub.com/cgi/doi/10.1177/0021998309343054

[8] P. Ladevèze, A damage computational method for composite structures, Computers and Structures 44 (1-2) (1992) 79–87. doi:10.1016/0045-7949(92)90226-P.

[9] O. Allix, P. Feissel, Composite Damage Model For Dynamic Fracture Prediction : Identification Issues, ICF 11-11th International Conference on Fracture 2005 (2005).

[10] L. J. Sluys, R. De Borst, Mesh-sensitivity analysis of an impact test on a double-notched specimen, Rock Mechanics, 1991 (1991).

[11] L. J. Sluys, R. de Borst, Wave propagation and localization in a rate-dependent cracked medium-model formulation and one-dimensional examples, International Journal of Solids and Structures 29 (23) (1992) 2945–2958. doi:10.1016/0020-7683(92)90151-I.

[12] L. F. Pereira, J. Weerheijm, L. J. Sluys, A new rate-dependent stress-based nonlocal damage model to simulate dynamic tensile failure of quasi-brittle materials, International Journal of Impact Engineering 94 (2016) 83–95. doi:10.1016/j.ijimpeng.2016.04.002.
URL http://dx.doi.org/10.1016/j.ijimpeng.2016.04.002

[13] T. Li Piani, J. Weerheijm, L. Koene, L. Sluys, The Adobe delta damage model: A locally regularized rate-dependent model for the static assessment of soil masonry bricks and mortar, Engineering Fracture Mechanics 206 (2019) 114–130. doi:10.1016/j.engfracmech.2018.11.026.
URL https://linkinghub.elsevier.com/retrieve/pii/S0013794418308956

[14] P. Ladeveze, E. LeDantec, Damage modelling of the elementary ply for laminated composites, Composites Science and Technology 43 (3) (1992) 257–267. doi:10.1016/0266-3538(92)90097-M.

[15] T. Li Piani, J. Weerheijm, L. Koene, L. J. Sluys, The Adobe Delta Damage Model, in: Computational Modelling of Concrete Structures (EURO-C 2018), CRC Press, Bad Hofgastein (Austria), 2018, pp. 921–932.

[16] T. Li Piani, J. Weerheijm, M. Peroni, L. Koene, G. Solomos, L. J. Sluys, Dynamic Characterization of Adobe in compression: The influence of fibre fraction in soil mixtures, in: FraMCoS-X : Fracture Mechanics of Concrete and Concrete Structures, Bayonne (France), 2019.

[17] P. Ladevèze, A damage computational approach for composites: Basic aspects and micromechanical relations, Computational Mechanics 17 (1995) 4–15. doi:10.1007/BF00356486.

[18] L. Pereira, J. Weerheijm, L. Sluys, A numerical study on crack branching in quasi-brittle materials with a new effective rate-dependent nonlocal damage model, Engineering Fracture Mechanics 182 (2017) 689–707. doi:10.1016/j.engfracmech.2017.06.019.
URL http://linkinghub.elsevier.com/retrieve/pii/S0013794417303028

[19] J. Lemaitre, J. Chaboce, Mechanics of Solid materials, 1990.

[20] J. Mazars, F. Hamon, S. Grange, A model to forecast the response of concrete under severe loadings : the nu damage model, Procedia Materials Science 3 (2014) 979–984. doi:10.1016/j.mspro.2014.06.159.
URL www.sciencedirect.com

[21] Z. liang Wang, Y. chi Li, R. F. Shen, J. G. Wang, Numerical study on craters and penetration of concrete slab by ogive-nose steel projectile, Computers and Geotechnics 34 (1) (2007) 1–9. doi:10.1016/j.compgeo.2006.09.001.

[22] J. Lee, G. L. Fenves, Plastic-Damage Model for Cyclic Loading of Concrete Structures, Journal of Engineering Mechanics 124 (8) (1998) 892–900. doi:10.1061/(ASCE)0733-9399(1998)124:8(892).
URL http://dx.doi.org/10.1061/(ASCE)0733-9399(1998)124:8(892){%}5Cnhttp://ascelibrary.org/doi/pdf/10.1061/(ASCE)0733-9399(1998)124:8(892)

[23] L. Pereira, J. Weerheijm, L. J. Sluys, Simulation of dynamic behaviour of quasi brittle materials with new rate dependent damage model, in: 9th International Conference on Fracture Mechanics of Concrete and Concrete Structures (FraMCos-9), 2015, p. 14. doi:10.21012/FC9.036.

[24] R. Ortiz, E. Deletombe, Y. Chuzel-Marmot, Assessment of damage model and strain rate effects on the fragile stress/strain response of ice material, International Journal of Impact Engineering 76 (2015) 126–138. doi:10.1016/j.ijimpeng.2014.09.011.
URL http://dx.doi.org/10.1016/j.ijimpeng.2014.09.011

[25] https://dianafea.com/manuals/d944/Analys/node435.html.

[26] V. P. Nguyen, Multiscale failure modelling of quasi-brittle materials. Manual to the implemented jem/jive code, Ph.D. thesis, Delft University of Technology (2011).
URL https://repository.tudelft.nl/islandora/object/uuid{%}3A1af168bf-7975-4044-8eb4-dd42216f7aaf

[27] JemJive libraries.
URL https://jive.dynaflow.com/

[28] L. J. Sluys, R. De Borst, Rate dependent modelling of concrete fracture, Heron 36(2), 3-16. (1991) (1992).

[29] L. F. Pereira, J. Weerheijm, L. J. Sluys, A new rate-dependent stress-based nonlocal damage model to simulate dynamic tensile failure of quasi-brittle materials, International Journal of Impact Engineering 94 (2016) 83–95. doi:10.1016/j.ijimpeng.2016.04.002.
URL http://dx.doi.org/10.1016/j.ijimpeng.2016.04.002

[30] L. J. Sluys, Wave Propagation, Localisation and Dispersion in Softening Solids, Ph.D. thesis, Delft University of Technology, TU Delft (1992).

[31] M. Jirásek, B. Patzák, Models for quasibrittle failure: Theoretical and computational aspects, ECCM-2001, European Conference on Computational Mechanics (2001) 70–71.

[32] K. Ravi-Chandar, An experimental investigation into dynamic fracture: I. Crack initiation and arrest, International Journal of Fracture 3 (4) (1984) 105–262. doi:10.1007/s00018-012-1041-2.

[33] P. D. Washabaugh, W. G. Knauss, A reconciliation of dynamic crack velocity and Rayleigh wave speed in isotropic brittle solids, International Journal of Fracture 65 (2) (1994) 97–114. doi:10.1007/BF00032282.

[34] J. K. Zhou, L. M. Ge, Effect of strain rate and water-to-cement ratio on compressive mechanical behavior of cement mortar, Journal of Central South University 22 (3) (2015) 1087–1095. doi:10.1007/s11771-015-2620-9.

[35] R. Pedersen, Computational modelling of dynamic failure of cementious materials, Ph.D. thesis, Tu Delft, Delft University of Technology (2010).

[36] P. H. Bischoff, S. H. Perry, Compressive behaviour of concrete at high strain rates, Materials and Structures 24 (6) (1991) 425–450. doi:10.1007/BF02472016.

[37] E. Cosenza, G. Maddaloni, G. Magliulo, M. Pecce, R. Ramasco, Seismic design of concrete structures (italian), Iuss Press, Pavia, 2007.

[38] R. Park, N. Pristley, W. Gill, Ductility of Square Confined Concrte Columns, in: Concrete Column Ductility, 1982.

[39] D. Silveira, E. al., Mechanical properties of adobe bricks in ancient constructions, Construction and Building Materials 28 (1) (2012) 36–44. doi:10.1016/j.conbuildmat.2011.08.046.
URL http://dx.doi.org/10.1016/j.conbuildmat.2011.08.046

[40] A. Suffis, T. A. A. Lubrecht, A. Combescure, Damage model with delay effect analytical and numerical studies of the evolution of the characteristic damage length, International Journal of Solids and Structures 40 (13-14) (2003) 3463–3476. doi:10.1016/S0020-7683(03)00153-7.

[41] P. Ladevèze, O. Allix, J. F. Deü, D. Lévêque, A mesomodel for localisation and damage computation in laminates, Computer Methods in Applied Mechanics and Engineering 183 (1-2) (2000) 105–122. doi:10.1016/S0045-7825(99)00214-5.

[42] O. Allix, J.-F. Deu, Delayed-Damage Modelling for Fracture Prediction of Laminated Composites under Dynamic Loading, Engineering Transactions 45 (1) (1997).
URL http://et.ippt.gov.pl/index.php/et/article/view/680

[43] H. W. Reinhardt, J. Weerheijm, Tensile fracture of concrete at high loading rates taking account of inertia and crack velocity effects, International Journal of Fracture 51 (1) (1991) 31–42. doi:10.1007/BF00020851.

[44] O. Lengliné, R. Toussaint, J. Schmittbuhl, J. E. Elkhoury, J. P. Ampuero, K. T. Tallakstad, S. Santucci, K. J. Måløy, Average crack-front velocity during subcritical fracture propagation in a heterogeneous medium, Physical Review E - Statistical, Nonlinear, and Soft Matter Physics 84 (3) (2011) 1–13. doi:10.1103/PhysRevE.84.036104.

[45] J. Ožbolt, J. Weerheijm, A. Sharma, Dynamic tensile resistance of concrete - Split hopkinson bar test, in: R. Y. J.G.M. Van Mier, G. Ruiz, C. Andrade, X. Z. (Eds) (Eds.), VIII International Conference on Fracture Mechanics of Concrete and Concrete Structures, no. February 2013, 2013.

[46] Q. H. Zuo, F. L. Addessio, J. K. Dienes, M. W. Lewis, A rate-dependent damage model for brittle materials based on the dominant crack, International Journal of Solids and Structures 43 (11-12) (2006) 3350–3380. doi:10.1016/j.ijsolstr.2005.06.083.

[47] A. Berezovski, G. A. Maugin, On the propagation velocity of a straight brittle crack, International Journal of Fracture 143 (2) (2007) 135–142. doi:10.1007/s10704-007-9053-x.

[48] H. W. Reinhardt, Concrete Under Impact Loading - Tensile Strength and Bond, Heron 27 (3) (1982).

[49] H. Hao, B. Tarasov, Experimental Study of Dynamic Material Properties of Clay Brick and Mortar at Different Strain Rates 8 (2) (2008) 117.
URL http://search.informit.com.au/documentSummary;dn=137784543477420;res=IELENG

[50] N. Ã. Gebbeken, S. Greulich, A. Pietzsch, Hugoniot properties for concrete determined by full-scale detonation experiments and flyer-plate-impact tests, International Journal of Impact Engineering 32 (2006) (2017) 2017–2019. doi:10.1016/j.ijimpeng.2005.08.003.

[51] CEB (Comite Euro-International du Beton) : CEB-FIP Model Code 1990.

[52] E. C. Simons, J. Weerheijm, L. J. Sluys, Simulating brittle and ductile response of alumina ceramics under dynamic loading, Engineering Fracture Mechanics (April) (2019) 106481. doi:10.1016/j.engfracmech.2019.05.013.
URL https://doi.org/10.1016/j.engfracmech.2019.05.013

[53] S. Wang, M. H. Zhang, S. T. Quek, Mechanical behavior of fiber-reinforced high-strength concrete subjected to high strain-rate compressive loading, Construction and Building Materials 31 (2012) 1–11. doi:10.1016/j.conbuildmat.2011.12.083.
URL http://dx.doi.org/10.1016/j.conbuildmat.2011.12.083